

Mercury recovered from smeared solution by the organo-mercury lyase enzyme revealed and detected by an *in-cell* radioactive analysis

K. Takamiya and Y. Morimoto

*Institute for Integrated Radiation and Nuclear Science,
Kyoto University*

INTRODUCTION: Methylmercury or organomercury are severe harmful compounds that cause neurological diseases represented by the Minamata disease. Some soil bacteria (such as *Desulfovibrio dusulfricans*) methylate inorganic mercury in seawater and pond freshwater, and then the food chain and body concentration are carried out to plankton, microorganisms and fish shellfish. In humans, in particular, since the binding mode between sulfur and mercury (Cys-S-Hg) of cysteine could not be distinguished from methionine at the methionine passage gate in the brain, it is impossible to block and avoid them into the brain. An accumulation of such toxic mercury causes nervous system poisoning. Therefore, purification of mercury-contaminated water and soil and mercury recovery has been desired since before. The most convenient method for purification and recovery against mercury contamination is a method as a chelated precipitate of EDTA, dimethyl captosuccinic acid (DMSA) or the others. However, this method merely aggregates and solidifies mercury compounds, and the inorganic mercurilization from them demands highly complicated chemical operation.

Recently, we succeeded in structural analysis of the mercury-bound form of an organomercury lyase B (MerB), in which one mercury was bound quantitatively per molecule even in additive of CH_3HgCl reagents (1). In other words, it has been shown that organic mercury molecules are incorporated into inorganic mercury and held in the enzyme in genetically modified *E. coli* over-expressing a large amount of the MerB. Therefore, it is thought that organic mercury in a cultivation medium could be recovered and mineralized into inorganic mercury by culturing the MerB-expression strain with high density (so called the bioremediation).

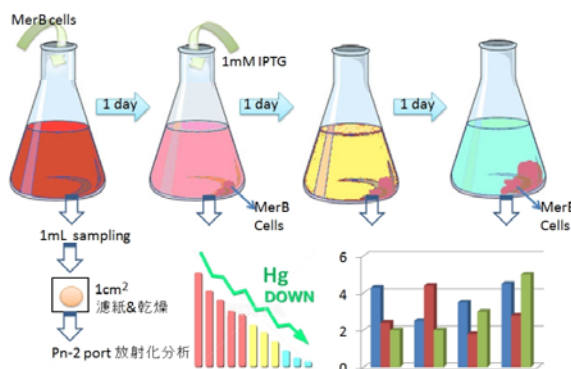


Fig.1 A schematic drawing of cultivation of the *E.coli* harboring MerB and medium sampling to radioactivation analysis

EXPERIMENTS: The enzyme was produced with an induction by isopropyl β -D-1-thiogalactopyranoside (IPTG) adding at the cell growth ($\text{OD } 650 = 0.6$). After this, MerB is accumulated in cells. During the sampling (Fig.1), 1 mL of medium is sampled, dried on filter paper, and used as a sample for neutron irradiation. Neutron irradiation and radioactive analysis at the irradiation port Pn-2 of the 5 MW research reactor (KUR) were carried out to which the applicant belongs. According to preliminary calculations, 500 ng Hg can be detected with 1 mL of filter paper dry-loaded with 1 mL of a medium containing mercury. The activation analysis is carried out by measuring γ -rays (279 keV) emitted with β -Decay of ^{203}Hg ($T_{1/2} = 46.6 \text{ d}$) generated by ^{202}Hg (n, γ) ^{203}Hg . Specifically, neutron irradiation is performed for 1 hour with a standard sample using PUR-2 of KUR, and after attenuating short half-life nuclide generated from impurities over about one week, γ -ray using Ge semiconductor spectrometry. The production amount of ^{203}Hg is estimated to be about 15 Bq, which can be measured with a statistical error of several% in about one day measurement. The amount of mercury is determined by a comparison method estimated from the ratio of the counting rate of the standard sample and the actual sample.

RESULTS and DISCUSSION: At 50 mL culture scale, methylmercury chloride was added to a concentration of 5, 2.5 mM, and with the progress of culture, the medium solution and the amount of cells were sampled, dried on filter paper, and used as a radioactive analysis sample.

Since a large amount of MerB is biosynthesized in the transformed cells during culture, methylmercury in the culture medium at the end of culture or during culture is cleaved along with the production of the enzyme molecule, and it is decomposed into mercury atoms to be digested inside the enzyme molecule. As a result of quantification after 96 hours considering the half life sufficiently, when the IPTG is not added (normal expression amount), the amount of mercury in the intracellular / medium is captured about twice as strongly, but IPTG induced cells, the ratio was reversed or equal and no significant difference was found. It is considered that the growth itself would be unstable in the transformed strain in which the enzyme molecule was forcibly expressed.

Acknowledgement: This work was supported by the Sumitomo Foundation 2017 and Kyoto Univ. education and research grant.

REFERENCES:

- 1) A study of preparation and structural analysis of the organomercury lyase for a neutron diffraction experiment. Y.Morimoto and A.Kita, Annual meeting of the KURRI 2017.

Y. Seki, T. Shinohara, M. Hino¹, T. Oda¹, Y. Matsumoto², J.D. Parker², T. Samoto³

J-PARC Center, JAEA

¹Institute for Integrated Radiation and Nuclear Science, Kyoto University

²Comprehensive Research Organization for Science and Society

³Institute of Multidisciplinary Research for Advanced Materials, Tohoku University

INTRODUCTION: Neutron phase imaging is an attractive method which can directly access the phase information of the neutron wave function, and investigate sensitively thinner or smaller structures of samples than by the conventional neutron radiography. We have been developing neutron phase imaging technique with the Talbot-Lau interferometer [1, 2], which consists of three gratings, at the Energy-Resolved Neutron Imaging System “RADEN” in J-PARC MLF.

One of the remarkable characteristics of the Talbot-Lau interferometer is attributed to the most upstream absorption grating (G0). G0 works as a multi-slit, and forms an array of spatially coherent line sources. Each source produces an interference pattern or a “moiré fringe” constructively through the middle phase grating (G1) and the most downstream absorption grating (G2). Therefore the Talbot-Lau interferometer is adaptable to even low-coherent and low-intensity beam of small- or middle-sized neutron sources.

For the spread of this method at such sources, we have developed a portable Talbot-Lau interferometry system and performed an imaging experiment at CN-3 beam line in Kyoto University Reactor (KUR). As the first step, typical visibility of moiré fringes and measurement precision at this beam line were studied by using a simple sample.

EXPERIMENTS: In the present experiment, we used a set of gratings which was fabricated for the RADEN beam line. The pitches of G0, G1, and G2 were 180 μm , 8.6 μm , and 9.0 μm , respectively. The distances from G0 to G1, and from G1 to G2 were 1534 mm and 76.5 mm, respectively. All the gratings were mounted on compact stage systems with pulsed-motors. As a neutron imager, the RPMT detector which consisted of a position-sensitive photomultiplier tube and a $\text{ZnS}^{60}\text{LiF}$ scintillator was employed behind G2.

The measurement was carried out by “phase-stepping method” as described below. First, a moiré fringe was scanned five times without the sample at the step of $2\pi/5$ rad by shifting the position of G2. From this measurement, the visibility of the moiré fringe was evaluated. Second, the same procedure was repeated with the sample. The measurement time was 40 min for each step, and totally $2 \times 5 \times 40 = 400$ min for one sample. By comparing the phase of two moiré fringes with and without the

sample, a differential-phase contrast image was obtained.

RESULTS: Fig. 1 shows a visibility map of the moiré fringe. The average visibility was 19% in the grating region. The relatively low visibility was observed because G1 was designed for the central wavelength of 5 \AA at the RADEN beam line which was quite different from the peak wavelength of 2.4 \AA at CN-3 beam line. The visibility distribution should be derived from mainly the thickness distribution of neutron absorber (gadolinium) on G2.

Fig. 2 shows a differential-phase contrast image of an aluminum rod with a diameter of 5 mm. The phase determination precision was about $2\pi \times 0.02$ rad with a pixel size of $0.22 \times 0.22 \text{ mm}^2$. By fitting a theoretical curve to the profile of the observed image, the effective wavelength, which reproduced the literature value of the optical potential of aluminum, was evaluated to be 2.55 \AA for differential-phase contrast imaging with this setup.

For more efficient measurement, we have a plan to fabricate new gratings in near future, which are optimized to the wavelength spectrum of CN-3 beam line.

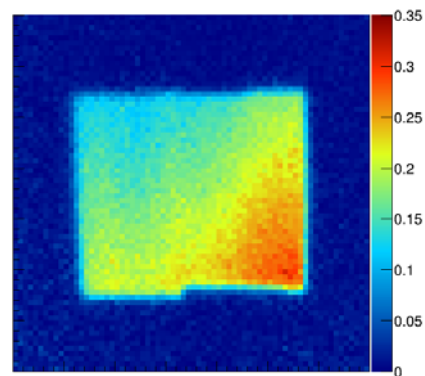


Fig. 1. Visibility map of moiré fringe.

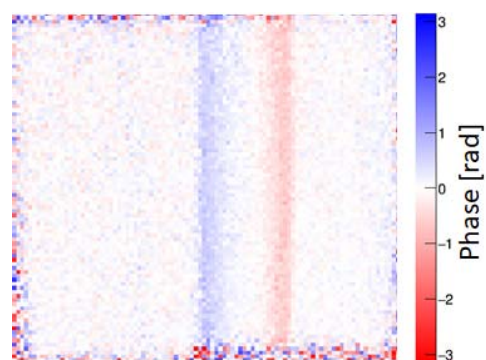


Fig. 2. Differential-phase contrast image of an aluminum rod.

REFERENCES:

- [1] Y. Seki *et al.*, J. Phys. Soc. Jpn., **86** (2017) 044001.
 [2] Y. Seki *et al.*, EPL, **123** (2018) 12002.

CO8-3 Test Result of Various Scintillator Sheet for Neutron Flat Panel Detector

T. Fujiwara¹ and M. Hino²

¹National Metrology Institute of Japan, National Institute of Advanced Industrial Science and Technology

²KURNS, Kyoto University

INTRODUCTION: Neutron imaging is powerful tool for observing inside an object without destructing the object. Although neutron imaging (neutron radiography) is one of the most traditional uses of neutrons, still there are rooms for improvement. Here, we report on the progress of neutron imaging result at reactor with our new neutron imaging detector based on Thin-Film-Transistor (TFT) technology, the neutron Flat Panel Detector. Various type of scintillators were tested for nFPD at neutron beam port at KUR.

EXPERIMENTS: Experiments were held in CN-3 port at Kyoto University Reactor [1]. At this facility, approximately $20 \times 100 \text{ mm}^2$ size cold neutron beam is available. Fig. 1 shows the outlook of the nFPD. The volume of the detector is remarkably compact and thin compared to the conventional neutron imagers. The size of this detector improves the flexibility for placing and it will be a great advantage for installation to various experiments. Meanwhile, nFPD only requires 5V (4W) single power supply, and simply connected to PC with USB cable. The detector has effective area with 512×512 pixels (200 mm pixel size).

In this experiment, we test 4 types of LiF/ZnS scintillators .

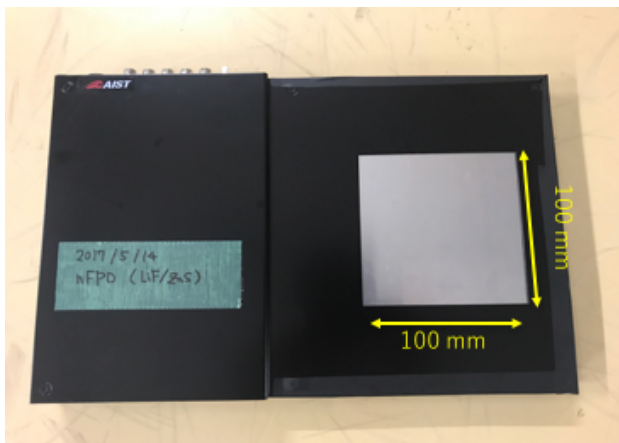


Fig. 1. Outlook of nFPD with $100 \times 100 \text{ mm}^2$ effective area. For the neutron convertor, 320 mm thick LiF/ZnS(Ag) scintillator was used.

RESULTS: First, simple neutron imaging capability of nFPD was tested with Gd coated test chart developed at PSI [2]. As shown in Fig. 2, fine neutron radiograph was

obtained. Fine structures less than $300 \mu\text{m}$ can be observed. From these results, it can be concluded as there are trade-off relationship between spatial resolution and the sensitivity of the scintillators.

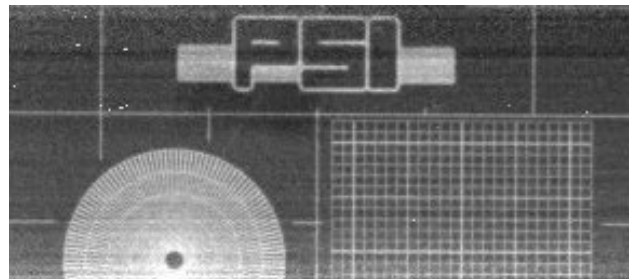


Fig. 2. Obtained neutron radiography of fine-structured Gd chart with nFPD. Integrating time was 5s at 1 MW operation. Fine patterns can be clearly observed.

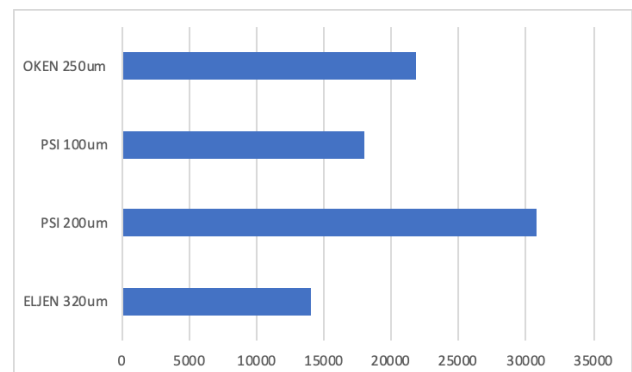


Fig. 3. Relative light output from various scintillators tested at CN-3.

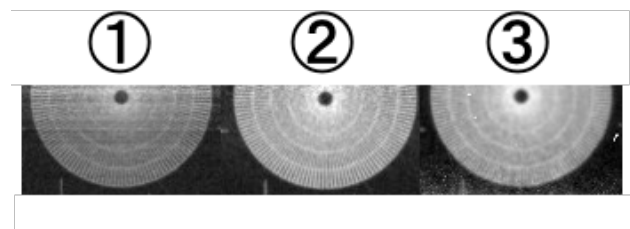


Fig. 4. Resolution comparison of various scintillators. (1) ELJEN Technologies EJ-426 $320 \mu\text{m}$ t, (2) OKEN 250 μm t, (3) PSI 200 μm t.

REFERENCES:

- [1] Y. Kawabata *et al.*, Physica B **311** (2002) 106.
- [2] K.-U. Hess *et al.*, Geosphere **7** 6. (2011) 1294-130.